The Generation of Optimal Microwave Topologies Using Time-Domain Field Synthesis

Mohamed H. Bakr, *Member, IEEE*, P. P. M. So, *Senior Member, IEEE*, and Wolfgang J. R. Hoefer, *Fellow, IEEE*

***Abstract*—We present a novel approach to the design of microwave structures using time-domain field synthesis. A standard transmission-line matrix (TLM) electromagnetic analysis of the starting geometry yields the structure response and the field distribution on the optimizable boundary parts. A number of characteristic frequencies equal to the number of designable parameters of the structure are determined first. For narrow-band structures, these frequencies may be natural resonance frequencies. For wide-band structures, we create appropriate resonance conditions. The target response of the structure allows us to identify the desirable values of these frequencies. For each parameter, a synthesis phase is then performed. In this phase, the optimizable boundary parts are replaced by matched TLM sources that inject sampled sinusoidal streams at the desired characteristic frequency. The TLM field model generates an electromagnetic field pattern. The synthesized geometry is obtained by examining the envelope of that field pattern. Our approach is illustrated by means of several examples.**

***Index Terms*—Computer-aided design (CAD), electromagnetic modeling, field-based synthesis, transmission-line matrix (TLM) method.**

I. Introduction

THE microwave structure design problem can be formulated as

$$\boldsymbol{x}^* = \arg\left\{ \min_{\boldsymbol{x}} U\big(\boldsymbol{R}(\boldsymbol{x})\big) \right\} \tag{1}$$

where $\boldsymbol{x}$ is the vector of designable parameters and $\boldsymbol{R}(\boldsymbol{x})$ is the vector of responses obtained by electromagnetic simulation. The designable parameters may include geometrical dimensions of the components. They may also include some material parameters such as substrate permittivities, etc. U is the objective function to be minimized and $\boldsymbol{x}^*$ is the vector of optimal designable parameters. U may be selected, if appropriate, as a generalized min–max objective function or L_2 objective function [1].

The classical approach for solving (1) treats the electromagnetic simulator as a black box. The derivatives of the responses are obtained through finite differences [1]. For a vector $\boldsymbol{x} \in \Re^n$, one optimization iterate involves $n+1$ full-wave simulations. This significant optimization toll motivates research for smarter optimization approaches.

Manuscript received June 18, 2001; revised December 2, 2001. This work was supported by the Natural Science and Engineering Council of Canada, by the University of Victoria, by Apollo Microwaves Ltd., by COM DEV Ltd., and by HeatWave Drying Systems Inc.

M. H. Bakr is with the Department of Electrical and Computer Engineering, McMaster University, Hamilton, ON, Canada L8S 4K1.

P. P. M. So and W. J. R. Hoefer are with the Computational Electromagnetics Laboratory, Department of Electrical and Computer Engineering, University of Victoria, Victoria, BC, Canada V8W 3P6.

Digital Object Identifier 10.1109/TMTT.2002.804522

Several efficient optimization approaches have been suggested. Space mapping [2] exploits the existence of another fast "coarse" model of the circuit under consideration. A mapping is established between the parameter spaces of the electromagnetic and coarse models. This mapping is then used to guide the optimization iterates. In [3], an analytical expression is derived for the admittance matrix of a finite-element analysis of a microstrip circuit. Another approach [4] derives the integral equation for the current derivatives. The derivatives are then expanded in terms of the same basis functions used in the analysis. The same LU decomposed analysis matrix is reused to solve for the derivatives coefficients.

The algorithm suggested in [5] exploits the time reversal property of the transmission-line matrix (TLM) method [6], [7]. The impulses corresponding to a desired response are obtained through inverse Fourier transform. These impulses are then propagated back in time to determine the geometry of the designable discontinuity. This inversion process does not always produce a unique geometry.

We suggest a novel approach for the synthesis of a microwave structure using the TLM method. The designable parameters are associated with a set of characteristic frequencies. These frequencies may either be natural resonance frequencies, poles, or zeros of responses or resonant frequencies created artificially in the band of interest by placing short or open circuits in the reference ports of a structure. The design specifications determine the desired values of these frequencies. A synthesis phase is then carried out for each parameter. In this phase, the corresponding optimizable boundary parts are replaced by matched TLM sources that inject a sampled sinusoidal signal at the characteristic frequencies. The field model is used to determine the new geometry by observing the envelope of the standing-wave field pattern in the structure.

We start with a brief review of TLM principles and of the time-reversal approach in Section II. Our novel approach is introduced in Section III. In Section IV, a number of simple examples are used to illustrate the algorithm. They have been selected to demonstrate the essence of the method rather than its ultimate potential. The examples include the design of a reentrant two-dimensional (2-D) cavity, an inductive post in a parallel-plate waveguide, and a single-resonator filter. Finally, conclusions are drawn in Section V.

II. TLM Method

The TLM method is a time- and space-discrete method for modeling electromagnetic waves. A mesh of interconnected transmission lines represents the propagation space. Developed and first published in 1971 by Johns and Beurle, it has emerged

as a powerful method for computer modeling of electromagnetic fields. The main advantage of the TLM simulation resides in the capability to model circuits of arbitrary geometry and to compute and display the time evolution of the fields. The TLM method exhibits excellent numerical stability and is also suitable for modeling lossy, dispersive, and nonlinear media.

In TLM, the continuous space is discretized by introducing a spatial network or mesh of TEM transmission lines. The electromagnetic field is represented by wave impulses scattered in the mesh nodes and propagating in the transmission lines linking the nodes. This model stresses the analogy between field and network concepts. Field components are modeled in terms of voltages and currents on the TLM network model. A detailed description and bibliography of the TLM is given in [7].

The TLM algorithm consists of two alternating processes, namely, the scattering of the wave impulses at the nodes and the transfer of the scattered impulses to the neighboring nodes. The wave amplitudes $\boldsymbol{V}_k^i$ incident on the nodes at the kth time step and the scattered-wave amplitudes $\boldsymbol{V}_k^r$ are related by the impulse scattering matrix $\boldsymbol{S}$

$$\boldsymbol{V}_k^r = \boldsymbol{S} \cdot \boldsymbol{V}_{\boldsymbol{k}}^i. \tag{2}$$

The impulses scattered from each node become incident on the neighboring nodes

$$\boldsymbol{V}_{k+1}^i = \boldsymbol{C} \cdot \boldsymbol{T} \cdot \boldsymbol{V}_k^r. \tag{3}$$

$\boldsymbol{C}$ is the connection matrix describing the mesh topology and $\boldsymbol{T}$ is the time-shift vector corresponding to the transit time Δt of the impulses between nodes.

A typical TLM electromagnetic analysis starts with the injection of one or several impulses into the TLM mesh. The impulses are then scattered according to (2) at each node in the computational domain. Impulses are also reflected at the boundaries with reflection coefficients that depend on the boundary properties. Scattered impulses travel to neighboring nodes during the time step Δt according to (3). The whole process is repeated for as many time steps as required.

The scattering matrix $\boldsymbol{S}$ is equal to its inverse [6]; this allows us to reverse the TLM process in time by simply exchanging the dependent and independent variables of the scattering equation without changing the scattering matrix, i.e.,

$$\boldsymbol{V}_k^i = \boldsymbol{S}^{-1} \cdot \boldsymbol{V}_k^r. \tag{4}$$

In a forward analysis, starting with a certain distribution of sources, the fields can be determined at all points for all time steps. In a backward analysis, we start with a certain field distribution (e.g., a desired field response) and propagate impulses back in time to get the initial source distribution. This includes the induced sources used to characterize the desired geometry of the circuit.

The reverse transmission-line matrix (RTLM) algorithm developed in [5] exploits this concept. However, the RTLM approach does not result in a unique design. It may lead to a structure different from the desired topology. In addition, the evanescent higher order modes required for defining the boundaries may not be accessible at the external absorbing boundaries within the frequency range of the discrete method used. This may reduce the resolution of the geometry. In Section III, we present our new algorithm as an alternative design approach.

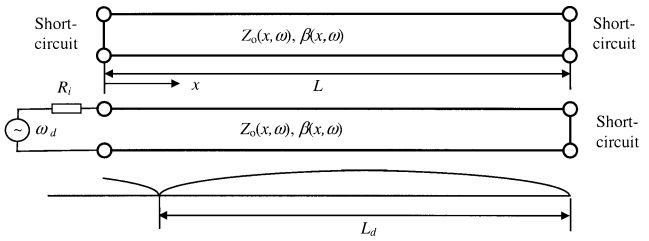

Fig. 1. (*top*) Length of a transmission-line resonator can be optimized by repeated analysis with different lengths L or (*bottom*) synthesized directly by injecting the resonant frequency into one end of the line and observing the standing-wave pattern.

III. Synthesis Procedure

We illustrate the basic concept of our novel synthesis procedure by considering a trivial, but fundamental example: the design of a $\lambda/2$ transmission-line resonator short-circuited at both ends (see Fig. 1). The characteristic impedance Z_o and the propagation constant β of the lossless line are not explicitly known and may be dependent on x and ω.

The specified (known) resonant frequency is ω_d, and the designable (hitherto unknown) parameter is L. ω_d is thus the characteristic frequency associated with the designable parameter L that must be determined such that the line resonates at ω_d.

If $\beta(x,\omega)$ of the line is not explicitly known, L cannot be synthesized analytically. Following the traditional optimization paradigm, one would select a starting value L_0 (first guess) and, by means of repeated analysis, find an optimal value L^* that minimizes the difference between its associated ω^* and the specified ω_d.

We propose instead to inject a sinusoidal time-dependent signal of frequency ω_d into one end of the transmission line. The standing-wave pattern on the line will yield the exact length L_d of the resonator in a single experiment or field analysis. Note that the source impedance R_i must not necessarily be matched to Z_o.

This method can be extended to 2-D and three-dimensional (3-D) situations by means of the TLM method. Consider the 2-D rectangular cavity shown in Fig. 2(a). It has been discretized by a TLM mesh with square cells. The length L is the designable parameter with a starting value L_0.

The situation is somewhat complicated by the fact that the field distribution is not uniform along the boundaries, and it may not be known *a priori* in the general case. We must, therefore, determine the correct field distribution in a first TLM analysis. By exciting the cavity with a band-limited signal containing its resonant frequency, we can establish a single-mode resonant field that yields the desired field distribution. Once the steady state is reached in the cavity, the TLM impulses incident on the left boundary $B(x)$ sample a sinusoidal signal of frequency ω_0, the resonant frequency of the cavity. Furthermore, each TLM link carries amplitude and phase information about the modal field distribution along $B(x)$. In our rectangular cavity, the impulse stream incident on $B(x)$ in the lth boundary link is given by

$$V_l^i(k\Delta t) = A_l \sin(k\omega_0 \Delta t + \theta_l) \tag{5}$$

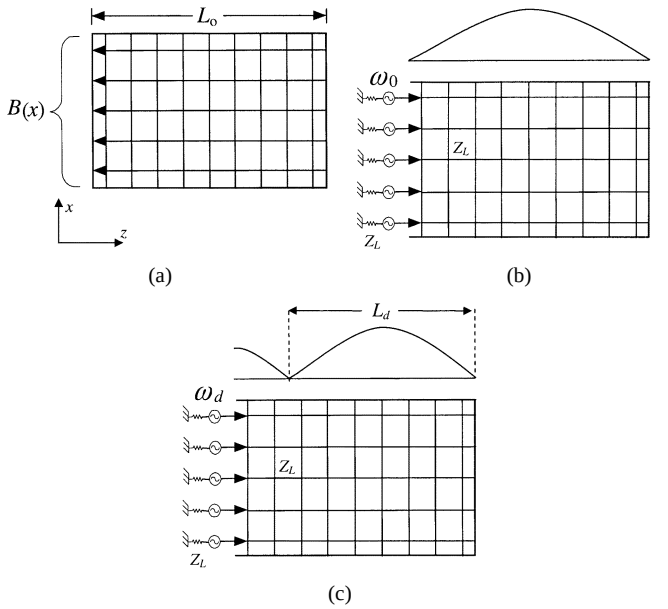

Fig. 2. Illustration of the algorithm for a single parameter L. (a) Standard TLM analysis where the impulses incident on $B(x)$ are stored. (b) Synthesis phase where $B(x)$ is replaced by matched sinusoidal impulse sources with frequency ω_0. (c) Synthesis phase with frequency $\omega_D > \omega_0$. The electric field points in the y-direction.

where l is an index for the link lines along the boundary, k is the discrete time variable, Δt is the time step, A_l is the amplitude, and θ_l is the zero phase angle. The boundary impulses given by (5) are reflected at the boundary with a reflection coefficient of -1. Note that, in our example, the amplitude A_l varies sinusoidally with x.

This situation is equivalent to that in Fig. 2(b), where the boundary part $B(x)$ is removed and replaced by TLM sources matched to the link line impedance Z_L of frequency $\omega = \omega_0$. The voltage of the lth source is

$$V_l(k\Delta t) = -2A_l \sin(k\omega\Delta t + \theta_l), \qquad \omega = \omega_0. \tag{6}$$

Note that we use the relative amplitudes and phases determined in the initial TLM analysis. The negative sign in (6) indicates that the sources represent the impulses reflected from $B(x)$ in Fig. 2(a). Also, the factor 2 in (6) is used because half of the source voltage drops across the source impedance. It follows that simulations based on the arrangements in Fig. 2(a) and (b) must yield identical fields in the cavity. The standing wave has a node line along $B(x)$.

In Fig. 2(c), we now change the frequency of the injected TLM impulse stream to $\omega = \omega_d > \omega_0$ while conserving the relative amplitudes and phases given in (6). During this TLM simulation, the node line in the cavity will be shifted toward the right due to the shorter guided wavelength, predicting the length required for the 2-D cavity to resonate at ω_d. This new length L_d has thus been synthesized directly.

The synthesis procedure can be generalized to cases with several designable parameters. Each designable parameter x_i will be associated with a characteristic frequency obtained from the design specifications. A standard TLM analysis of a starting geometry determines the structure response and yields the relative amplitudes and phases of impulses incident on the parts of the boundary that will be modified (without loss of generality, we limit ourselves to the case where $B(\boldsymbol{x})$ is a perfect conducting boundary). For each parameter x_i, a synthesis phase is then carried out during which $B(x_i)$ is replaced by matched TLM sources injecting a sampled sinusoidal signal with the desired value of the associated characteristic frequency. To avoid the excitation of spurious modes, a Gaussian-ramped sinusoidal excitation of the following form can be used:

$$\begin{aligned} V_l(k\Delta t) &= A_l \sin(k\omega_d\Delta t + \theta_l) e^{-((k-k_m)^2/(2k_\sigma^2))}, \qquad k \le k_m \\ V_l(k\Delta t) &= A_l \sin(k\omega_d\Delta t + \theta_l), \qquad k > k_m. \end{aligned} \tag{7}$$

Here, l is an index of the TLM link lines bounded by $B(x_i)$. The parameters A_l, θ_l, and ω_d are the relative amplitude, relative phase, and frequency of the injected sinusoidal signal, respectively. The parameters k_m and k_σ are such that the bandwidth of the excitation contains a single mode.

By injecting the signal at the boundary part $B(x_i)$, only one degree of freedom is allowed for the modified structure. The field model finds the desired boundary position within the constraints imposed by the starting geometry. This position is obtained by examining the steady-state field envelope patterns

$$E_{\max}(i,j) = \max_{k>k_s} |E(i,j,k)|$$

and/or

$$H_{\max}(i,j) = \max_{k>k_s} |H(i,j,k)|. \tag{8}$$

k is the time index, while i and j are the indexes of the nodes in the x- and z-directions, respectively. k_s is the steady-state time index. A new location of an electric wall is determined by a minimum of the tangential electric-field component. Similarly, the position of a magnetic wall can be determined by finding a minimum of the tangential magnetic field. By virtue of the physical properties of electromagnetic fields, this design procedure also minimizes the losses and the sensitivity to tolerances.

It should be noted that the values of the designable parameters are determined, through interpolation or extrapolation, with a higher precision than the grid size Δl. However, to verify the design, the values of the parameters are usually snapped to the grid.

Our approach can be summarized by the following algorithm steps.

Step 1) Initialize $i = 1, \boldsymbol{x}^{(i)}, \delta^{(i)}$ and obtain $\boldsymbol{R}(\boldsymbol{x}^{(1)})$.
Comment: In the case of a resonant cavity, we have $\boldsymbol{R}(\boldsymbol{x}) \in \Re^1$ and $\boldsymbol{R}(\boldsymbol{x}) = \omega(\boldsymbol{x})$, the resonant frequency. For an open structure, we may use $\boldsymbol{R}(\boldsymbol{x}) \in \Re^m$, where $R_i(\boldsymbol{x}) = S_{11}(\omega_i), i = 1, 2, \ldots, m$ and m is the number of simulation frequencies. $\delta^{(i)}$ is the size of the trust region used to limit the step taken.

Step 2) Obtain the characteristic frequencies corresponding to the desired response $\boldsymbol{R}_d$.

Step 3) Perform the synthesis phase for each $x_j, j = 1, 2, \ldots, n$ to get $\Delta\boldsymbol{x}^{(i)}$.
Comment: Notice that $\Delta\boldsymbol{x}^{(i)}$ may be scaled to satisfy $\|\Delta\boldsymbol{x}^{(i)}\| \le \delta^{(i)}$.

Step 4) Obtain $\boldsymbol{R}(\boldsymbol{x}^{(i)} + \Delta\boldsymbol{x}^{(i)})$ using TLM electromagnetic analysis.

Step 5) If $U(\boldsymbol{R}(\boldsymbol{x}^{(i)} + \Delta\boldsymbol{x}^{(i)})) \le U(\boldsymbol{R}(\boldsymbol{x}^{(i)}))$, let $\boldsymbol{x}^{(i+1)} = \boldsymbol{x}^{(i)} + \Delta\boldsymbol{x}^{(i)}$. Otherwise $\boldsymbol{x}^{(i+1)} = \boldsymbol{x}^{(i)}$.

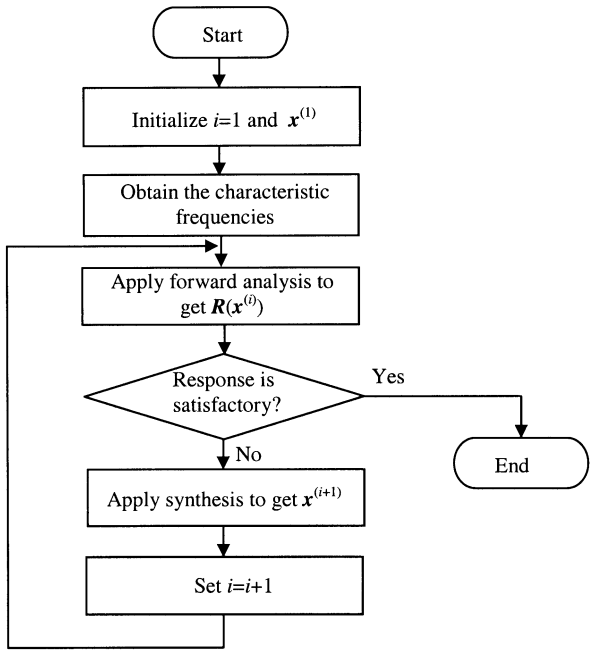

Fig. 3. Flowchart of the synthesis algorithm.

Comment: The objective function is taken as $U(\boldsymbol{R}(\boldsymbol{x}^{(i)})) = ||\boldsymbol{R}(\boldsymbol{x}^{(i)}) - \boldsymbol{R}_d||$.

Step 6) If $U(\boldsymbol{R}(\boldsymbol{x}^{(i)})) \leq \varepsilon$ or $\|\Delta \boldsymbol{x}^{(i)}\| \leq \varepsilon$ Stop.

Step 7) Update $\delta^{(i)}$, set $i = i + 1$ and go to Step 3.

Note that the algorithm allows for more than one optimization iterate if the desired response is not obtained in just one step. A flowchart of the algorithm is shown in Fig. 3.

IV. Examples

The one-dimensional (1-D) and 2-D resonator examples discussed above are rather straightforward. The 2-D resonator is amenable to exact analytical treatment, and we have verified that, in this case, the field synthesis procedure is accurate within the second-order modeling error of the TLM mesh. To demonstrate that the procedure also works for more complex narrow-band and wide-band microwave structures, we present three more examples, namely, a reentrant resonator, an inductive waveguide discontinuity, and a simple waveguide bandpass filter.

A. Synthesis of a Reentrant Resonator

Fig. 4(a) shows the geometry of a 2-D reentrant resonator. We assume that the electric field is normal to the cross section and, hence, tangential to the conducting sidewalls. The optimizable parameter is the length L. All other dimensions are fixed at $a = 30$ mm, $b = 51$ mm, and $W = 5$ mm. We select a starting value $L_0 = 7.0$ mm, discretize the structure with a 1.0-mm TLM grid, and inject a band-limited signal containing the dominant resonant frequency ω_0. The resulting steady-state electric field pattern at resonance is shown in Fig. 4(b). During this first analysis, we store all TLM impulses incident upon the optimizable boundary $B(L)$ from the five link lines bounded by it [see Fig. 4(c)]. We can now proceed to the synthesis procedure.

After replacing the boundary $B(L)$ with matched sources [see Fig. 4(d)], we inject the desired resonant frequency while preserving the relative amplitudes and phases of the impulse streams stored during the analysis phase. Since the sources absorb all impulses incident upon $B(L)$, a steady-state field will establish itself in the resonator after some time. Fig. 5(a) shows the electric-field profile along the symmetry axis normal to $B(L)$ for three values of the injected frequency. Extrapolation of these curves yields the corresponding values of L. Fig. 5(b) compares the predicted value of the dimensional ratio $\alpha = L/L_0$ with the value obtained by subsequent TLM analysis for different frequency ratios $r = \omega_d/\omega_0$. Obviously, the extrapolation is easier and more accurate if the design frequency ω_d is higher than the initial value ω_0 since the field node then falls within the computational domain. Again, the extrapolation can be performed with higher resolution than the grid size. Furthermore, a second iteration can be performed if the first guess for L_0 was too far off.

If the difference between the initial and synthesized values of L is larger than the mesh size, the lateral boundaries of the reentrant notch are not adjusted during the synthesis phase and, consequently, the synthesized field pattern has a node line that is not parallel to $B(L)$, but looks like the contour shown in Fig. 6. Here, we have made the notch somewhat larger ($W = 7\Delta l$) to show this effect more clearly. The smooth profile is, in fact, optimized in the sense that it minimizes the field energy stored around the face of the notch, thus suggesting a boundary profile that reduces the risk of field breakdown and also minimizes conductor losses if the boundaries are not lossless.

B. Synthesis of an Inductive Obstacle in a Waveguide

The next example demonstrates the synthesis of a centered inductive post in a parallel-plate waveguide (see Fig. 7). The post is much thinner than the wavelength and can thus be represented by a lumped equivalent T circuit for frequencies up to the cutoff of the first higher mode in the guide.

If we want to synthesize the width W and thickness D so that the post has specified equivalent reactances jX_c and jX_l (or specified frequency-dependent S-parameters), we must first identify a characteristic frequency associated with each of the optimizable parameters W and D. By placing electric walls (short circuits) at a distance L from the post, we create a resonator that can sustain even and odd resonant modes (see Figs. 8 and 9). The general resonance conditions for these modes are

$$S_{11}^d(\omega_e) + S_{21}^d(\omega_e) = -e^{2j\beta_e L} \tag{9}$$

and

$$S_{11}^d(\omega_o) + S_{21}^d(\omega_o) = -e^{2j\beta_o L} \tag{10}$$

where e and o stand for "even" and "odd," respectively. The odd mode accommodates a short circuit in the A–A'-plane and, thus, its resonant frequency depends mainly on the value of D. The even mode accommodates an open circuit in the A–A'-plane, and its resonant frequency depends essentially on W.

Our goal is to synthesize the dimensions W and D of the post in a parallel-plate waveguide of width $a = 60$ mm. Its target S-parameter response is shown in Fig. 9(b). For this example, we have generated the target response by analyzing, with the TLM, a post with $W = 10$ mm and $D = 5$ mm. Our procedure will allow us to synthesize these values from this response.

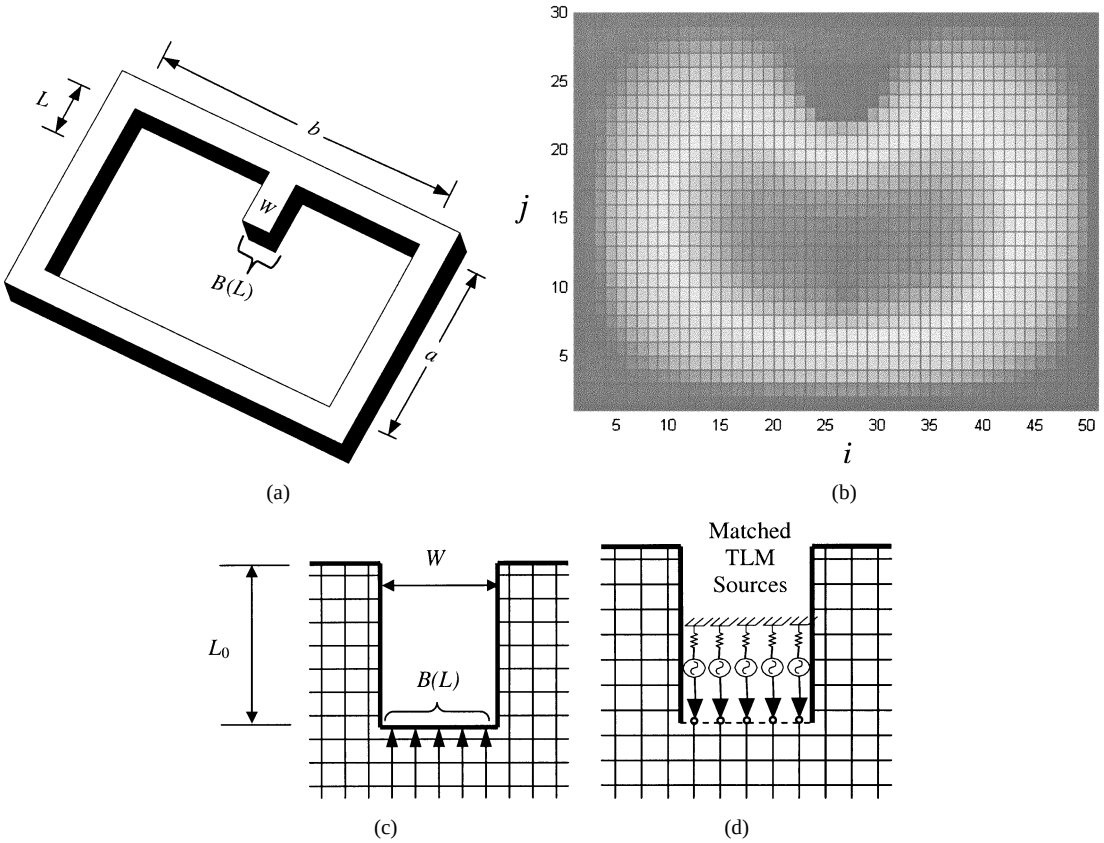

Fig. 4. (a) Reentrant resonator. (b) The envelope of the steady-state electric field in the discretized reentrant resonator for $L = L_0$. The mesh size is 1 mm × 1 mm. (c) Detail of the TLM mesh in the vicinity of the optimizable boundary $B(L)$ where the incident TLM impulses are stored. (d) Matched TLM sources inject the stored TLM impulses after shifting the frequency of their envelope to the desired value.

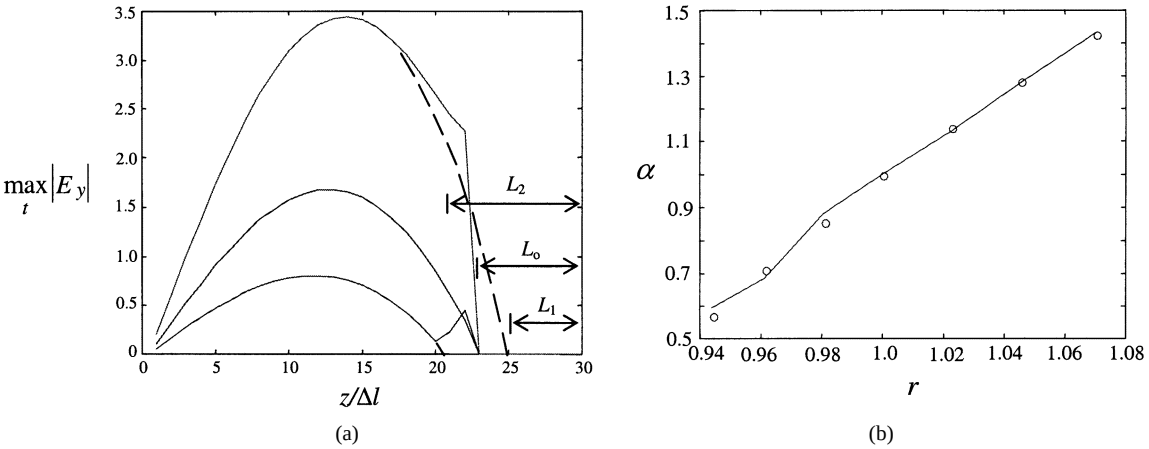

Fig. 5. (a) Electric-field envelope pattern obtained for different values of the injected frequency. The corresponding values of L are found by extrapolation. (b) The value of the dimensional ratio α versus the frequency ratio r for the reentrant resonator. (o) = values predicted by synthesis, $(—)$ = TLM analysis.

As mentioned earlier, we must begin with the TLM analysis of an approximate structure. We choose as start values $W_0 = 6$ mm and $D_0 = 4$ mm. To create the even- and odd-mode resonators, we must also choose a value for L such that the near field at the discontinuity is not perturbed, and that the even and odd resonant frequencies are below cutoff of the first higher mode in the waveguide. Once L is selected, the target even and odd resonant frequencies can be obtained by solving the transcendental equations (9) and (10) using the specified target S-parameters. The choice of $L = 60$ mm yields the following target resonant frequencies.

- Even target resonant frequency: $f_{0e} = 2.0075$ GHz.
- Odd target resonant frequency: $f_{0o} = 2.5255$ GHz.

However, the initial TLM analysis of the resonator with start values $W = 6$ mm and $D = 5$ mm yields the following resonant frequencies.

- Even initial resonant frequency: $f_{1e} = 1.8873$ GHz.
- Odd initial resonant frequency: $f_{1o} = 2.5174$ GHz.

While the resonant frequencies obtained by the initial TLM analysis are off target, the amplitudes and phases of the TLM impulse streams incident upon the optimizable boundaries

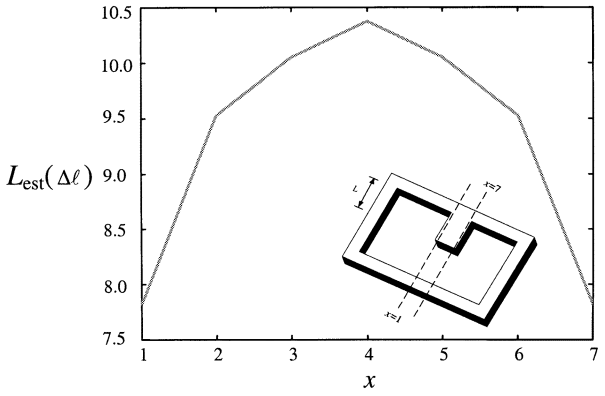

Fig. 6. Node line of the synthesized field pattern in the cross-sectional plane for the case $W = 7$ mm. This boundary contour would minimize energy stored at the notch face.

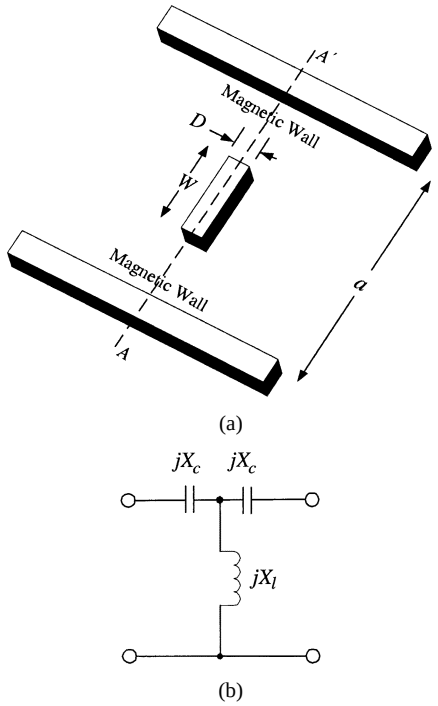

Fig. 7. (a) Geometry of an inductive post in a parallel-plate waveguide with magnetic sidewalls. (b) Its equivalent lumped-element representation.

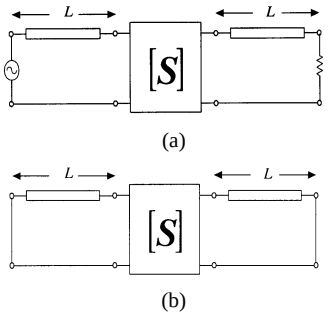

Fig. 8. Symmetric and reciprocal lossless two-port network representing the inductive post. (a) Arrangement for regular S-parameter evaluation. (b) Resonator created by shorting the input and output sections at distance L from the post.

are virtually identical to those incident at the target resonant frequencies. After recording these amplitudes and phases, we inject impulse streams at the even and odd target frequencies

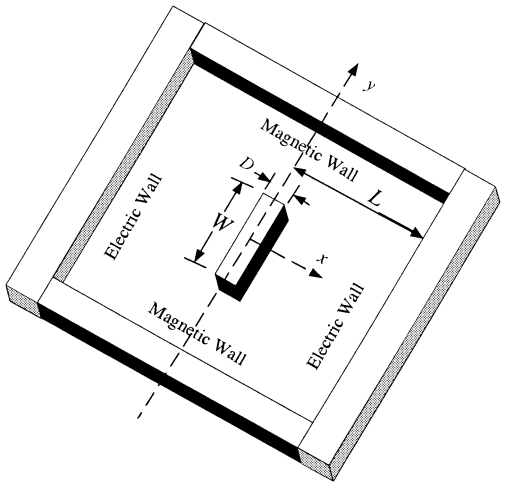

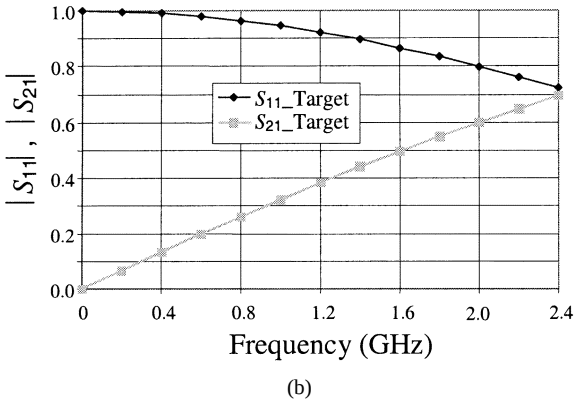

Fig. 9. (a) Resonator created by shorting the reference ports of the inductive post. (b) Target S-parameter response of the post in a 60-mm-wide parallel-plate guide.

normal to D and W, respectively, using matched TLM sources, as shown in Fig. 4. The resulting standing-wave patterns are shown in Figs. 10 and 11. Extrapolation of the field profiles yields the exact specified post dimensions with a single simulation per optimizable parameter. If the difference between the initial guess and final dimensions is very large, a second iteration can be performed to improve accuracy, a measure that is not necessary in this example.

C. Single-Resonator Filter

We have also synthesized the single-resonator filter shown in Fig. 12. The designable parameters are W and d. The width of the waveguide is fixed at $a = 60$ mm. The starting geometry is taken as $d = 36$ mm and $W = 15$ mm. All walls are perfectly conducting boundaries.

The target S-parameters are supplied by the equivalent circuit shown in Fig. 13. This circuit features ideal transmission lines and an empirical model of the discontinuity [8]. MATLAB[1] simulates the circuit as a cascade of uncoupled sections [9]. The target response along with the initial response is shown in Fig. 14.

The characteristic frequency associated with d is the resonant frequency of the cavity formed by placing electric walls in the

[1]The Math Works Inc., Natick, MA 01760.

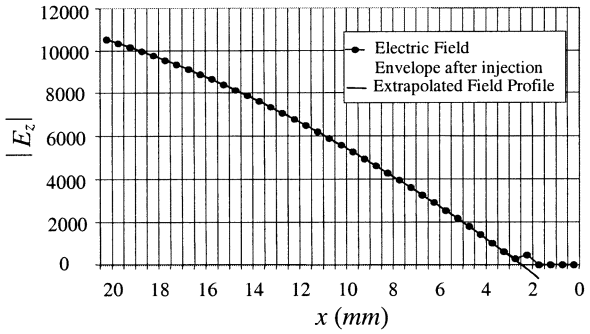

Fig. 10. Electric-field envelope along the x-axis after injection of the odd resonant target frequency at the end walls of the obstacle. The sources are located at $x = 2$ mm. (Only one-half of the symmetrical cross section is shown.)

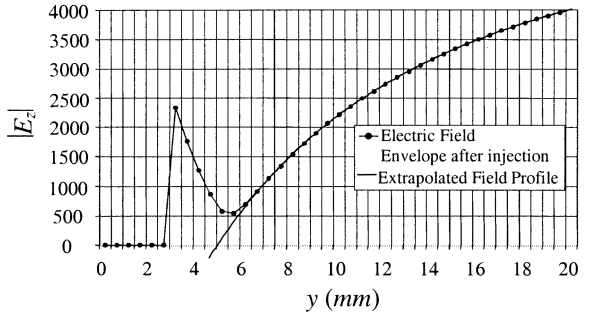

Fig. 11. Electric-field envelope along the y-axis after injection of the even resonant target frequency of 2.0075 GHz at the sidewalls of the obstacle. The sources are located at $y = 3$ mm (Only one-half of the symmetrical cross-section is shown.)

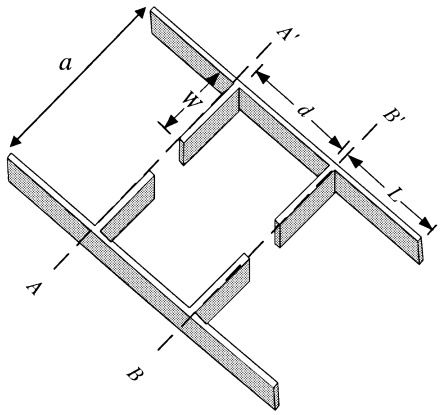

Fig. 12. Topology of the single-resonator filter.

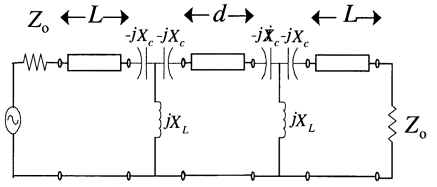

Fig. 13. Equivalent-network model of the single-resonator filter.

planes AA' and BB'. This frequency is the resonant frequency of the midsection of the circuit in Fig. 13 when a short circuit is placed across the two shunt inductances, and it can be obtained from the equivalent circuit in Fig. 13. We inject that frequency

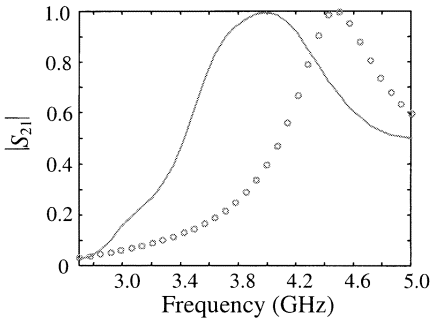

Fig. 14. Target response (o) and the initial response $(—)$ of the single-resonator filter.

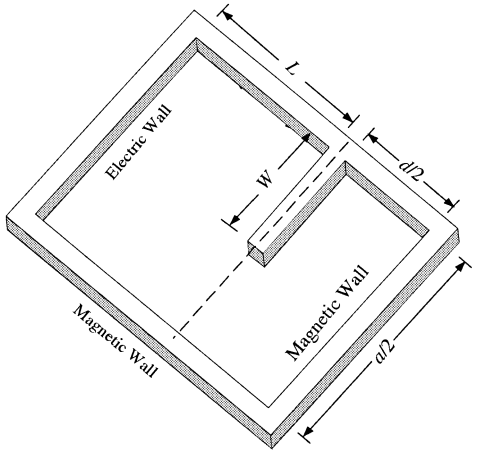

Fig. 15. One-fourth of the single resonator.

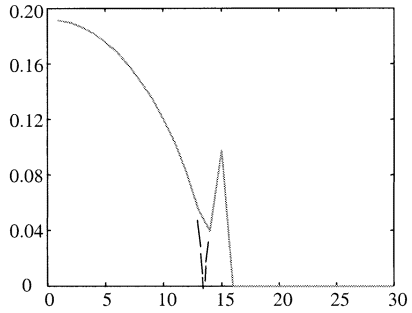

Fig. 16. Field envelope pattern for the outer cavity of the single-resonator filter along the discontinuity width.

with a sinusoidal transverse source distribution at the left- or right-hand side of a rectangular cavity, as discussed previously. Note that we can reduce the computational effort by taking advantage of symmetry. We obtain a synthesized cavity length of $d = 30$ mm.

The characteristic frequency associated with W is the even-mode resonant frequency of the cavity generated by shorting the input and output ports. We utilize the symmetry properties of the even mode and use only one-fourth of the structure in the synthesis phase (see Fig. 15). The envelope of the electrical field, observed along the discontinuity plane, is shown in Fig. 16. The desired width of the discontinuity, snapped to the grid, is thus $W = 18$ mm. The final response of the filter is shown in Fig. 17. A good match with the target response is obtained.

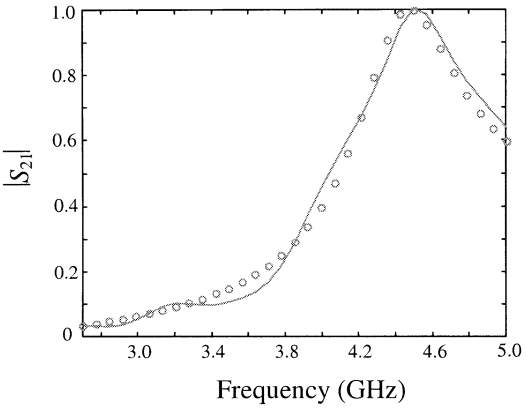

Fig. 17. Target response (o) and the final response (—) of the single-resonator filter.

V. Conclusion

The foundations of a novel approach to microwave structure design has been presented. We have utilized electromagnetic-field synthesis to determine the desired geometry. Each designable parameter has been associated with a characteristic frequency of the structure. For each parameter, a synthesis phase has been performed at the corresponding characteristic frequency. The field envelope patterns have then been examined to predict the modified geometry. Our approach has been successfully tested through a number of examples. The approach will be extended to more complex synthesis scenarios in the future.

References

[1] J. W. Bandler, W. Kellermann, and K. Madsen, "A superlinearly convergent minimax algorithm for microwave circuit design," *IEEE Trans. Microwave Theory Tech.*, vol. MTT-33, pp. 1519–1530, Dec. 1985.

[2] M. H. Bakr, J. W. Bandler, K. Madsen, J. E. Rayas-Sánchez, and J. Søndergaard, "Space mapping optimization of microwave circuits exploiting surrogate models," in *IEEE MTT-S Int. Microwave Symp. Dig.*, Boston, MA, 2000, pp. 1785–1788.

[3] P. Garcia and J. P. Webb, "Optimization of planar devices by the finite element method," *IEEE Trans. Microwave Theory Tech.*, vol. 38, pp. 48–53, Jan. 1990.

[4] J. Ureel and D. De Zutter, "A new method for obtaining the shape sensitivities of planar microstrip structures by a full-wave analysis," *IEEE Trans. Microwave Theory Tech.*, vol. 44, pp. 249–260, Feb. 1996.

[5] M. Forest and W. J. R. Hoefer, "A novel synthesis technique for conducting scatterers using TLM time reversal," *IEEE Trans. Microwave Theory Tech.*, vol. 43, pp. 1371–1378, June 1995.

[6] R. Sorrentino, P. P. M. So, and W. J. R. Hoefer, "Numerical microwave synthesis by inversion of the TLM Process," in *21st Eur. Microwave Conf. Dig.*, Stuttgart, Germany, 1991, pp. 1273–1277.

[7] W. J. R. Hoefer, "The transmission-line matrix method-theory and applications," *IEEE Trans. Microwave Theory Tech.*, vol. MTT-33, pp. 882–893, Oct. 1985.

[8] N. Marcuvitz, *Waveguide Handbook*, 1st ed. New York: McGraw-Hill, 1951.

[9] R. E. Collin, *Foundations for Microwave Engineering*. New York: McGraw-Hill, 1992.

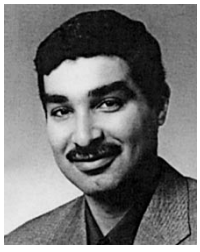

Mohamed H. Bakr (S'98–M'00) received the B.Sc. degree (with distinction) in electronics and communications engineering and the Master's degree in engineering mathematics from Cairo University, Cairo, Egypt, in 1992 and 1996, respectively, and the Ph.D. degree in electrical and computer engineering from McMaster University, Hamilton, ON, Canada, in 2000.

In 1997, he was an Intern with Optimization Systems Associates (OSA) Inc. From 1998 to 2000, he was a Research Assistant with the Simulation Optimization Systems (SOS) Research Laboratory, McMaster University. In November 2000, he joined the Computational Electromagnetics Research Laboratory (CERL), University of Victoria, Victoria, BC, Canada, as a National Sciences and Engineering Research Council of Canada (NSERC) Post-Doctoral Fellow. He is currently an Assistant Professor with the Department of Electrical and Computer Engineering, McMaster University.

Dr. Bakr held the Ontario Graduate Scholarship (OGS) for two consecutive years (1998–2000). He was the recipient of a 2000 NSERC Post-Doctoral Fellowship. His research areas of interest include optimization methods, CAD and modeling of microwave circuits, neural-network applications, smart analysis of microwave circuits, and efficient optimization using time-domain methods.

P. P. M. So (S'86–M'88–SM'00) is currently an Adjunct Assistant Professor and Senior Research Engineer with the Department of Electrical and Computer Engineering, University of Victoria, Victoria, BC, Canada. From April 1997 to June 1998, he was a Senior Antenna Engineer with EMS Canada Ltd. (formerly Spar Aerospace Ltd.). His work has included high-frequency (10–40 GHz) antenna and feed component design for commercial satellite systems, as well as Ka-band active antenna CAD software development. In October 1993, he was invited to the Ferdinand-Braun-Institut fur Hochstfrequenztechnik Berlin, Berlin, Germany, as a Research Scientist. From August 1990 to February 1991, he was a Visiting Researcher with the University of Rome, Rome, Italy, and the Laboratoire' d'Electronique, Sophia Antipolas, France. During his time abroad, he developed a number of electromagnetic wave simulators for the Digital MPP and Connection Machine CM2 massively parallel computers. Since 1998, he has authored or coauthored over 30 refereed journal and conference papers and coauthored *The Electromagnetic Wave Simulator—A Dynamic Visual Electromagnetics Laboratory Based on the Two-dimensional TLM Method* (New York: Wiley, 1991). He is a reviewer for the Wiley *International Journal of Numerical Modeling—Electronic Networks, Devices and Fields*. He is a co-founder of the Faustus Scientific Corporation and the President and C.E.O. of the WiseThought Software Corporation, Victoria, BC, Canada. He is also the creator and chief software architect of the `MEFiSTo` line of products of the Faustus Scientific Corporation.

Dr. So is a member of the Editorial Board for the IEEE TRANSACTIONS ON MICROWAVE THEORY AND TECHNIQUES for the computational electromagnetics and CAD areas.

Wolfgang J. R. Hoefer (M'71–SM'78–F'91) received the Dipl.-Ing. degree in electrical engineering from the Technische Hochschule Aachen, Aachen, Germany, in 1965, and the D.Ing. degree from the Universitaire de Technologie de Grenoble, Grenoble, France, in 1968.

During the 1968–1969 academic year, he was a Lecturer with the Institut Universitaire de Technologie de Grenoble, and a Research Fellow with the Institut National Polytechnique de Grenoble, Grenoble, France. In 1969, he joined the Department of Electrical Engineering, University of Ottawa, Ottawa, ON, Canada, where he was a Professor until March 1992. Since April 1992, he holds the National Sciences and Engineering Research Council of Canada (NSERC) Industrial Research Chair in Radio Frequency Engineering with the Department of Electrical and Computer Engineering, University of Victoria, Victoria, BC, Canada. In 1976–1977, during sabbatical leaves, he spent six months with the Space Division of AEG–Telefunken (now ATN), Backnang, Germany, and six months with the Electromagnetics Laboratory, Institut National Polytechnique de Grenoble. He has subsequently been a Visiting Scientist with the Space Electronics Directorate, Communications Research Centre, Ottawa, ON, Canada, and a Visiting Professor with the University of Rome "Tor Vergata,"Rome, Italy, University of Nice–Sophia Antipolis, Nice–Sophia Antipolis, France, and Technical University of Munich (TUM), Munich, Germany. He is the President of the Faustus Scientific Corporation. He is the co-founder and Managing Editor of the *International Journal of Numerical Modeling*. His research interests include numerical techniques for modeling electromagnetic fields and waves, CAD of microwave and millimeter-wave circuits, microwave-measurement techniques, and engineering education.

Dr. Hoefer is a Fellow of the Advanced Systems Institute of British Columbia.